Journal of Alloys and Compounds 815 (2020) 152334

Contents lists available at ScienceDirect

Journal of Alloys and Compounds

journal homepage: http://www.elsevier.com/locate/jalcom

Solidification behaviour of undercooled equiatomic FeCuNi alloy

M.R. Rahul, Gandham Phanikumar*

Department of Metallurgical and Materials Engineering, Indian Institute of Technology Madras, Chennai, 600036, India

ARTICLE INFO

Article history:
Received 22 April 2019
Received in revised form
10 September 2019
Accepted 17 September 2019
Available online 18 September 2019

Keywords:
Undercooling
Dendritic growth velocity
Phase field simulation
Segregation
Equiatomic alloys

ABSTRACT

Studies on solidification of equiatomic multi-component alloys are essential in developing melt-route processing of high entropy alloys. The extent of undercooling during processing controls microstructure evolution. In this study, we present solidification studies on undercooled equiatomic FeCuNi alloy carried out using melt fluxing technique. The alloy shows a two-phase (FCC + FCC) microstructure even at deep undercooling of more than 200 K. The dendrite growth velocity measured using high-speed video imaging shows a nonlinear increase in growth velocity with the increase in the extent of undercooling. A modified dendritic growth model was able to predict the growth velocity. The segregation behaviour and microstructures at different extents of undercooling can be predicted using phase field simulation.

1. Introduction

Development of multi-component alloys with equiatomic composition has seen rapid growth in recent years due to the search for remarkable properties [1–3]. Multi-component equiatomic alloys are designated as high entropy alloys based on the configurational entropy of a random solid solution of the constituent elements. Understanding the solidification behaviour of equiatomic multi-component alloys can improve upon the design of high entropy alloys. This is because segregation during solidification can lead to undesirable precipitates that could limit the application of an alloy arrived through combinatorial designs and equilibrium thermodynamic estimates.

Solidification studies using the extent of undercooling as a control parameter are useful in determining microstructure evolution during manufacturing processes including those that involve non-equilibrium conditions such as additive manufacturing [4]. The number of studies on phase selection kinetics or morphological changes in the multicomponent alloys during undercooled conditions is limited in the open literature [5–7].

The ternary equiatomic alloys such as CoCrNi gained attraction due to their mechanical properties and unique mechanisms [8,9]. Alloying with titanium, carbon [10] and tungsten [11] have shown improvement in strength and other properties of this alloy. However, studies on the effects of undercooling on ternary alloys are limited to the corners of the respective phase diagrams [12–14]. Given the rapid growth in the number of studies on equiatomic multicomponent/high entropy alloys, undercooling studies on alloys at the centre of the phase diagram need exploration to aid in the development of novel microstructures.

The data on dendrite growth velocity as a function of undercooling can be used to predict the underlying mechanisms of microstructure formation during solidification. The dominance of a particular component of undercooling (from thermal, solutal, curvature and kinetic components) often provides insights into the mode of solidification. The growth velocity as a function of undercooling can be predicted based on the material parameters including thermodynamic and kinetic data using established dendrite growth models [15–17]. The prediction of microstructural evolution using phase field modelling can be used to identify the segregation of elements in regions away from the tip of the dendrite. Studies have shown that phase field simulations match experimental results in case of ternary Ni–Al–Zr system in the undercooled condition [14]. Quantification of segregation could help avoid conditions that lead to the formation of undesirable intermetallic compounds while designing high entropy alloys. An integrated approach that combines thermodynamic and kinetic calculations guiding the experiments could help in the design of novel high entropy alloys [18].

Functional applications such as the giant magnetic resistance (GMR) have used the FeCuNi system with non-equiatomic compositions [19]. Undercooling studies on binary systems Fe-Cu [20]

* Corresponding author.
E-mail address: gphani@iitm.ac.in (G. Phanikumar).

https://doi.org/10.1016/j.jallcom.2019.152334
0925-8388/

and Cu–Ni are reported in the literature [21–23]. The studies on Cu–Ni and Fe–Ni systems show different grain refinement mechanisms in different undercooling regimes [24,25]. The Fe–Cu system shows a submerged miscibility gap leading to metastable liquid phase separation at critical undercooling. This phenomenon is sensitive to the composition of the alloy system. The undercooling studies on Cu–Ni system show the transition from dendritic to equiaxed grains and the effect of recrystallisation during solidification is also studied [23]. From the high entropy alloy reports, it can be concluded that the HEAs with Fe, Cu, Ni elements are studied mainly in multiphase as well as eutectic alloy development [26–28]. Alloy systems such as FeCoNiCuNb [27], FeCoNiCuMn [26] and FeCoNiCuCrAl [29] are reported in literature. The equi-atomic FeCuNi ternary is a derivative in these systems. The undercooling studies on FeCoNiCuCr system showed growth velocity of the order of ~2 m/s at an undercooling of 200 K [30] which is lower than Ni based alloys. There exists a controversy whether the growth rates in equiatomic multicomponent alloys is sluggish or not. On the way to understand the growth kinetics in multi-principle element alloy with several components, we need to explore ternary equiatomic systems as well. Undercooling studies on ternary equiatomic systems will help in understanding growth kinetics as well as microstructure evolution in HEAs with multiple elements.

In this study, the equiatomic alloy Fe–Cu–Ni was chosen to understand the solidification behaviour and growth velocity as a function of undercooling. Data on the growth velocity as a function of undercooling were measured experimentally and correlated with dendritic growth models. Multi-phase field approach was used to predict the segregation pattern in the alloy during the undercooled condition.

1.1. Experimental details

As-cast sample was prepared using a vacuum arc melting technique with tungsten as a non-consumable electrode. The starting materials were high purity elements (>99.99) and melted in an inert atmosphere. The alloy was remelted several times flipping each time to homogenise the composition across the sample. The remelted alloy sample of 25 g weight was sectioned using electric-discharge machining to obtain samples of required weight for metallographic preparation and undercooling study. The undercooling experiments using melt fluxing technique were carried out under argon atmosphere. The flux used was boron trioxide. The born trioxide flux will cover the sample and this liquid/amorphous layer will avoid the contact of sample with the container and thereby prevents any nucleation sites from being available to the melt. By avoiding nucleation sites, the melt is able to undercool below the liquidus temperature before crystallization could initiate. During the experiments, the sample holding temperature was around 200 K above the liquidus before quenching with the inert gas to obtain undercooling. The thermal profile of the solidifying sample was captured using a two-colour infrared pyrometer (Impac®) to an accuracy of ±5 K. The high-speed video images (Photron FASTCAM® (SA4) with SIGMA® lens attachment) were captured from the sample during solidification at a frame rate of 10^5 per second. Thermal contrast was adequate in determining the recalescence speed by image analysis using PFV® (Photron FASTCAM Viewer) software.

The metallographic preparation was performed using emery polishing followed by colloidal silica solution. The structural characterisation was carried out using X-ray diffraction (XRD) (using X'pert Pro PANalytical® with Cu-$K_\alpha$radiation of wavelength $\lambda = 0.154056$ nm). The microstructure characterisation included scanning electron microscopy (InspectF® and Quanta400®, FEI make) in backscattered electron mode, local composition measurements using energy dispersive spectroscopy (EDS) (using Oxford EDAX®), and transmission electron microscopy (using Tecnai-FEI® with EDAX® attachment) for an independent phase confirmation. DSC (SETARAM Labsys®) measurements were carried out using an as-cast sample of 55 mg weight and heating is done by a rate of 10 K/min.

1.2. Simulation details

Microstructure simulation of solidification after different extents of undercooling was performed using MICRESS® software that implements a multi-phase field model. The simulation parameters used are shown in Table 1. The use of thermodynamic data in the simulation was by enabling TQ coupling with Thermo-Calc® software. The input diffusion data assumed the primary phase to be a solid solution of Fe. The microstructural simulation was carried out using a reduced multiphase field equation for solidification [14,31,32] as shown below

$$\frac{\partial \Phi}{\partial t} = \mu^*(\vec{n})\left[\sigma^*(\vec{n})\left(\nabla^2\Phi + \frac{\pi^2}{\eta^2}\left(\Phi - \frac{1}{2}\right)\right) + \frac{\pi}{\eta}\sqrt{\Phi(1-\Phi)}\,\Delta G\right]$$

where Φ is the phase field order parameter, $\mu^*(\vec{n})$ is the anisotropic interfacial mobility, η is the diffuse interface thickness, $\sigma^*(\vec{n})$ is the anisotropic interfacial energy, and ΔG is the Gibbs energy as driving force. The realistic simulation was achieved due to the TQ coupling with the thermodynamic database (TCHEA 2). The simulated segregated profiles taken as virtual line EDS were validated against the experimentally determined line-scan profiles.

2. Results and discussion

2.1. As-cast microstructure

The phase evolution predicted by using Thermo-Calc® (TCHEA 2 database) in Scheil's regime is shown in Fig. 1a. This confirms the formation of FCC single phase as also observed in the as-cast microstructure. The DSC curve shown in Fig. 1b confirms the liquidus temperature viz., 1638 K which is close to the thermodynamic prediction of 1623 K. The error in the measured and predicted liquidus temperature was around 1% which could indicate further improvement in database is necessary for a more accurate prediction. The SEM-EDS image shown in Fig. 1c shows that the as-cast microstructure consists of Fe–Ni rich primary dendritic phase and Cu rich interdendritic region. The EDS map shows the complete depletion of Fe from the Cu rich region and Cu from the Fe–Ni rich region. This is expected from the largely positive enthalpy of mixing and resultant immiscible nature of Fe and Cu. The TEM micrograph shown in Fig. 2a and b confirms that Cu rich region and Fe–Ni rich region are dis-ordered FCC phase. Composition measured by EDS was shown in Table 2. The Cu rich region consists of nanoscale precipitates shown in the inset image. The presence of fine Fe–Ni rich precipitates is of significance to applications related to GMR effect [19]. The role of metastable extended solid solution and subsequent phase separation leading to the nanoscale Fe precipitates cannot be ruled out. The precipitations in Fe–Cu alloys due to undercooling (which is also common in fast processes such as laser scanning) are reported earlier [33,34]. The precipitates are local segregation of elements – ie., iron in copper-rich regions and copper in iron-rich region. Such microstructures are known from alloy systems that exhibit submerged miscibility gap. Also, there are several studies that have established copper segregation in steels and their role in improving the strength [35,36]. From the

Table 1
Parameters used for phase field simulation.

Parameter	Value and Unit
Diffusion constant of Cu in the melt	2.4×10^{-5} cm^2/s
Diffusion constant of Cu in the dendrite	2.4×10^{-10} cm^2/s
Diffusion constant of Ni in the melt	6.01×10^{-6} cm^2/s
Diffusion constant of Ni in the dendrite	6.01×10^{-10} cm^2/s
Kinetic coefficient (μ) between phases, liquid and primary dendritic phase [cm^4/(Js)]	30.00000×10^{-04}
Surface energy between phases, liquid and primary dendritic phase [J/cm^2]	1.00000×10^{-05}
Domain size, Grid size	600×600 μm, 0.3 μm

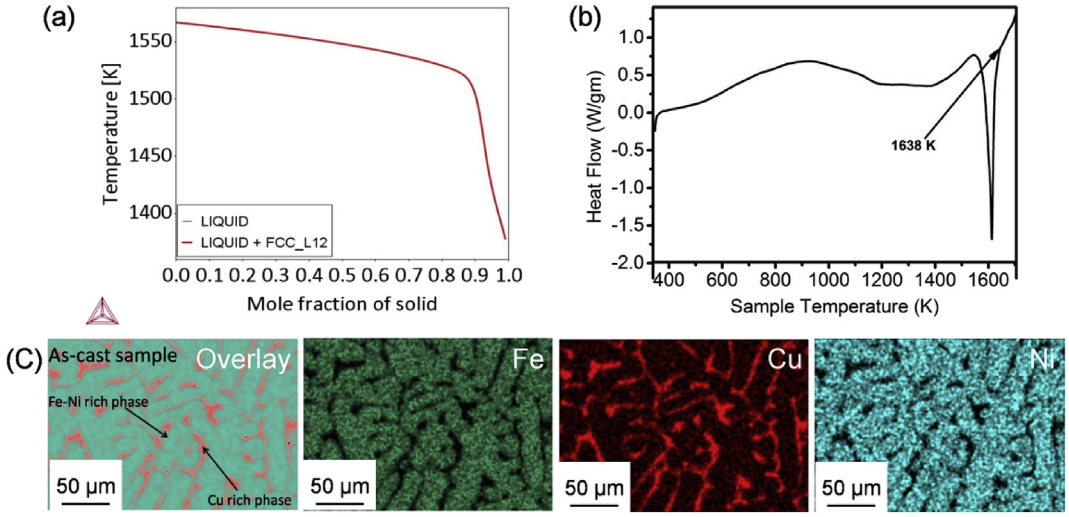

Fig. 1. a) Scheil's solidification pathway predicted by Thermo-Calc®, b) Differential Scanning Calorimetry (DSC) curve shows the liquidus temperature of alloy, c) Scanning electron microscopy (SEM) image with EDS mapping of as cast sample.

length scale of these precipitates, we believe that these are formed in solid state during the cooling portion of the thermal cycle.

2.2. Thermal profile characteristics

Fig. 3 shows a superposition of thermal profiles of different undercooling experiments. The extent of undercooling is estimated as the difference between the liquidus temperature and the recalescence temperature. The rise in temperature due to latent heat evolution is not sufficient to raise the temperature above the liquidus temperature at undercooling $\Delta T > 95$ K. The thermal profiles show only one recalescence event which corresponds to the primary Fe—Ni rich dendrite phase. The plot also confirms that there is no other phase transformation at different levels of undercooling.

2.3. Characterisation of undercooled samples

Fig. 4 shows the microstructures of samples solidified at different extents of undercooling (ΔT). At low undercooling regime ($\Delta T < 36$ K) the microstructure consists of Fe—Ni rich dendritic structure with Cu rich interdendritic region. The dendritic structure was primarily due to diffusion-controlled growth during solidification where the dendritic growth velocity expected to be lower. At higher undercooling, the microstructure exhibits a refinement. The microstructure consists of Fe—Ni rich primary phase and Cu rich interdendritic region in all undercooling regimes.

In the undercooling range $36 \text{ K} < \Delta T < 62$ K, the primary Fe—Ni rich regions show polycrystalline morphology. This appearance is due to the dendritic remelting that occurs during the recalescence. Thermo-solutal remelting of dendrites is also likely – given the formation of finally solidified Cu rich region surrounding the Fe—Ni rich region. If the liquid fraction during the remelting is more than 0.8, it could cause the remelting of the initially formed dendritic skeleton and lead to refinement of the microstructure [25]. In the case of Fe—30Ni, the liquid fraction is more than 0.8 in the regime of undercooling less than 100 K. The morphology variation in a different regimes is reported for Cu—Ni system [24].

In the regime of undercooling $62 \text{ K} < \Delta T < 211$ K, the microstructure shows columnar dendritic morphology. In this regime, the dendrite remelting is not expected because of higher undercooling. The proportion of liquid will be less than 80% as in Fe—Ni system reported in the literature [25]. At an undercooling of $\Delta T > 211$ K, the microstructure consists of grain morphology which is possibly due to recrystallisation following an increase in strain during solidification and dendrite distortion. The volume change during solidification could lead to increased stored energy in the solid and result in recrystallisation. This type of grain refinement was observed in Fe—30Ni as well as Cu—Ag and Ni-based alloys [24,25,37]. Reduced segregation of Cu at the grain boundaries corroborates such a possibility. The transformation may be due to the dominance of thermal and kinetic undercooling in higher undercooling regime compared to the solute diffusion dominated lower undercooling regime.

The microstructure did not exhibit liquid phase separation unlike in undercooled binary Fe—Cu systems [20]. The extended solution of Ni in both Fe and Cu in elevated temperature may result in the avoidance of submerged miscibility gap even in higher undercooling conditions. At high undercooling, the length scale of the Cu rich interdendritic region decreased due to the solute trapping unlike in the case of Fe—Cu system. From this microstructure

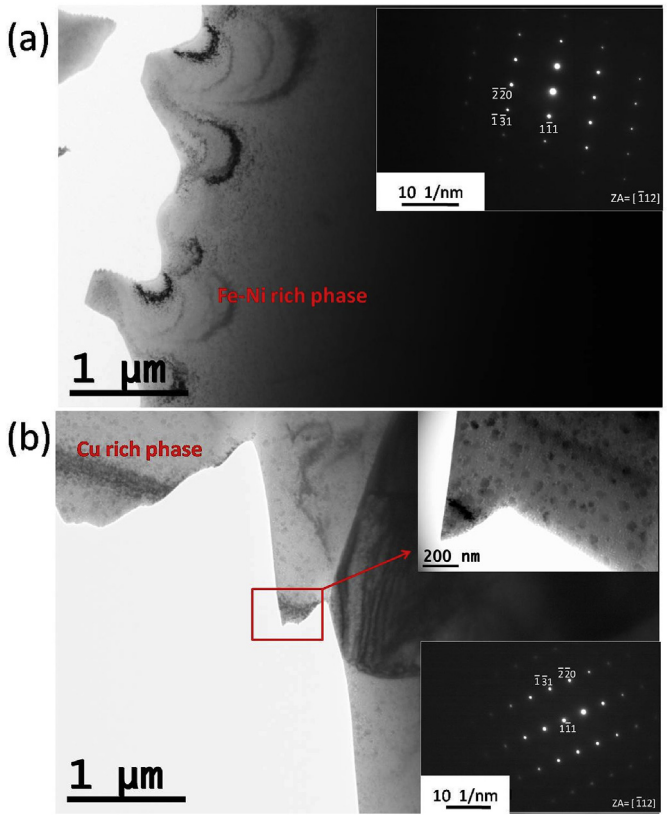

Fig. 2. Transmission electron microscopy (TEM) bright field image shows a) Fe–Ni rich FCC phase with SAED pattern of zone axis [ī12] in the inset, b) Cu rich FCC phase with SAED pattern of zone axis [ī12] in the inset and the red rectangle shows the magnified region with precipitates, The EDS composition of different region was shown in Table 2. (For interpretation of the references to colour in this figure legend, the reader is referred to the Web version of this article.)

Table 2
Composition of different phases measured by EDS.

Elements	FeNi rich phase (atomic %)	Cu rich phase (atomic %)
Fe	39.68	9.20
Ni	37.03	10.46
Cu	23.29	80.34

evolution, one can state that the Fe–Cu–Ni equiatomic alloy exhibits two-phase microstructure without metastable phase separation. The morphological changes suggest dominated by two different grain refinement mechanisms at low and high undercooling regimes.

Structural characterisation using XRD (Fig. 5) confirms the FCC phase in the as-cast as well as deeply undercooled samples. The Cu rich phase has a lattice parameter close to that of Fe–Ni rich phase and leads to an overlap of peaks in the XRD pattern.

2.4. Dendrite growth velocity

The growth velocity was calculated based on the high-speed video imaging by tracking the motion of the recalescence front (Fig. 6a and b). The thermal contrast images show that in the low undercooling regime, the recalescence front is angular and at higher undercooling regime the recalescence front is smooth (spherical) in morphology. Such a transition from angular to smooth recalescence front was known in the Ni system [38] and is applicable in the Fe–Cu–Ni system as well. The transition from

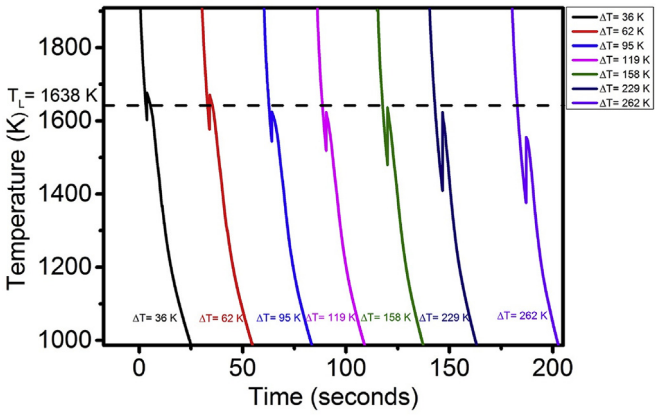

Fig. 3. Thermal profile of undercooling experiments.

angular recalescence front to a smooth recalescence front was at the undercooling range of 140 K–162 K.

The dendritic growth velocity exhibits the expected trend of an increase with undercooling. The velocity shows a steep increase in the high undercooling regime and is attributed to the dominant thermal undercooling contribution. High velocity in higher undercooling regime leads to polycrystalline or grain morphology of microstructure. Grain morphology due to recrystallisation was reported in Fe–Ni system when the growth velocity is more than 25 m/s [25]. In the equiatomic Fe–Ni–Cu alloy, the grain morphology was observed at undercooling ($\Delta T > 211$ K) that corresponds to a velocity of more than 25 m/s condition. It is possible that the mechanism for grain morphology is similar in this system too. The growth velocity obtained was comparable to the Ni and Fe based alloys [21,39]. The variation of growth velocity (V) can be fitted to a nonlinear function of undercooling as follows

$$V = 0.00889(\Delta T)^{1.48}$$

The bulk undercooling obtained experimentally is a sum of contributions from solutal, thermal, curvature, and kinetic undercooling. In the low undercooling regime the solutal effect is dominant, and in the high undercooling regime the kinetic and thermal contribution is dominant. This can be observed in other binary [40,41] as well as ternary systems, in case of Ni–Fe–Si system, it was reported that the diffusion-controlled growth was prominent at lower undercooling which is due to solutal undercooling. The collision controlled growth is dominant at the higher undercooling condition which is due to kinetic and thermal undercooling [42]. Fe–Ge system shows that the fraction of solutal and curvature undercooling was more than 0.6 around 150 K undercooling which suggested that diffusion is more prominent in the lower undercooling regime [43]. The models used for each undercooling contribution are described in detail elsewhere [43]. The formulation used in the current studies is presented briefly here.

The bulk undercooling achieved by the sample can be written as

$$\Delta T = \Delta T_t + \Delta T_s + \Delta T_k + \Delta T_r \quad (1)$$

Where each term will the contribution to the total undercooling. Thermal undercooling which is dominant at higher undercooling region mainly due to the temperature gradient with the solid-liquid interface and the rest of the sample can be written as

$$\Delta T_t = \Delta T_{hyp} Iv(P_t) \quad (2)$$

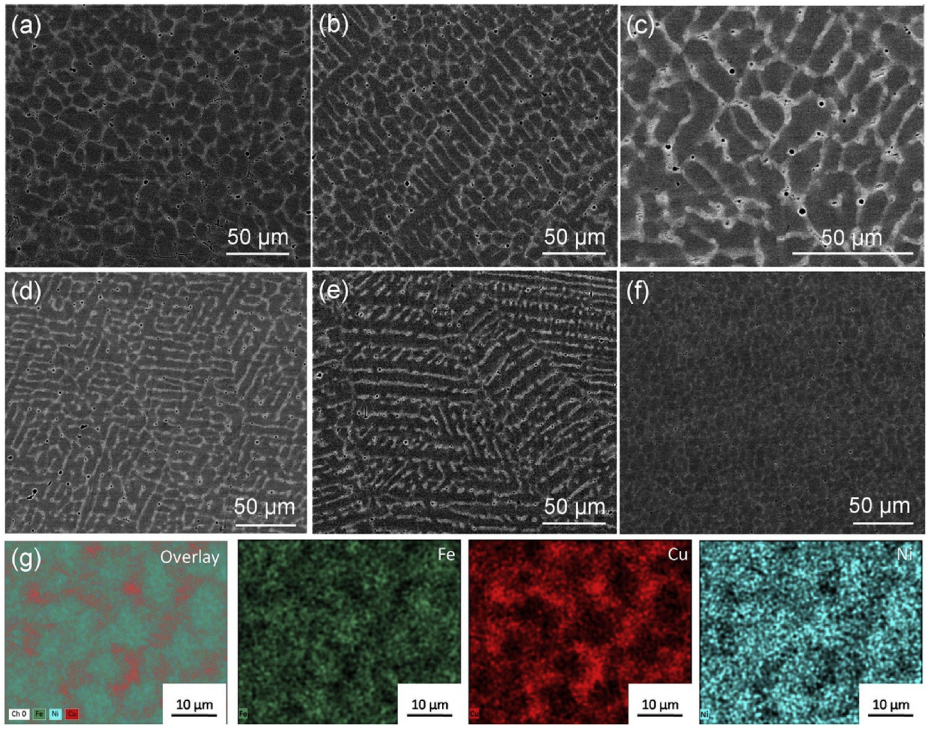

Fig. 4. Scanning electron microscopy- Backscattered electron images of undercooled sample at various level of undercooling a) $\Delta T = 36$ K, b) $\Delta T = 62$ K, c) $\Delta T = 95$ K, d) $\Delta T = 119$ K, e) $\Delta T = 158$ K, f) $\Delta T = 262$ K and g) EDS mapping of $\Delta T = 262$ K sample at higher magnification.

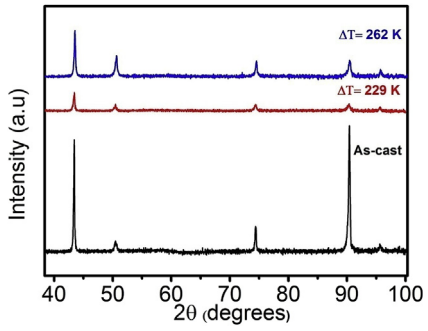

Fig. 5. XRD pattern of as cast and undercooled samples.

Where the terms ΔT_{hyp} is hypercooling $= (\Delta H/C_i)$, ΔH is latent heat of fusion and C_i is heat capacity of liquid, $Iv(P_t)$ is the Ivantsov function, the thermal Peclet number is expressed as P_t. The undercooling due to solute rejection at the interface can be expressed as solutal undercooling

$$\Delta T_s = mC_o\left\{1 - \left\{\frac{\frac{m'}{m}}{1-(1-k)Iv(Pc)}\right\}\right\} \quad (3)$$

where liquidus slope is m, was obtained from the phase diagram generated using Thermo-Calc® with TCHEA2 database and m' = slope of kinetic liquidus can be found from the equilibrium partition coefficient and k is the velocity-dependent partition coefficient and solutal Peclet number expressed as P_c. The undercooling due to the curvature of the dendritic tip can be expressed as curvature undercooling

$$\Delta T_r = 2\Gamma / r \quad (4)$$

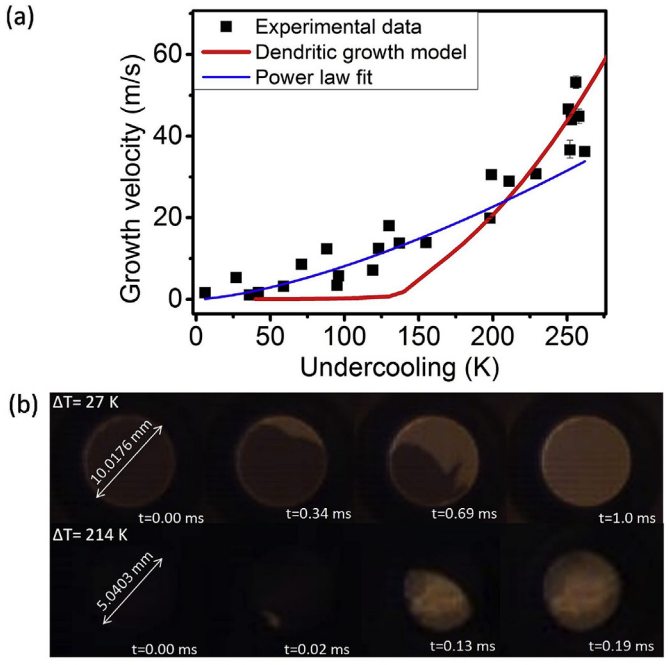

Fig. 6. a) Shows growth velocity variation with respect to undercooling from experimental data and dendritic growth theory. b) High speed video imaging shows the solid-liquid interface where bright area is solid and dark area is liquid (At $\Delta T = 27$ K the diameter of sample is 10.0176 mm and at $\Delta T = 214$ K the diameter of sample is 5.0403 mm).

Where Γ is Gibbs-Thomson coefficient and r is the dendritic tip radii.

A modification in the kinetic undercooling contribution of the dendrite growth model allowed for a closer correlation with the

measured variation of growth rate as a function of undercooling. The non-linear kinetic contribution similar to an earlier study [43] is taken as follows:

$$\Delta T_k = \mu\left(\frac{v}{v_C}\right)^p$$

The model assumed a pseudo-binary approach considering mainly Fe(Ni) as the primary solution phase and Cu as the major segregating element. The parameters used for the calculation are shown in Table 3. The extent of non-linearity modelled using the parameter p given in the kinetic undercooling term was taken to be 0.7 for this system, and V_c is the maximum growth rate at the infinite driving force, and μ is the kinetic coefficient. The hypercooling value was calculated from Thermo-Calc® database TCHEA2 using the latent heat of solid and liquid at the liquidus and specific heat of liquid at the liquidus. The estimation of the pseudo-binary partition coefficient of Cu was from the compositions in the as-cast sample. Solute diffusivity values were taken from the literature, and remaining parameters are optimised to fit with the experimental results [43,44]. The discrepancy between the predicted growth rates and experimentally measured data could be attributed to the original dendrite growth model being for dilute alloys, apart from uncertainties in different parameters. However, the qualitative agreement indicates that solidification of undercooled equiatomic alloys could also be modelled using dendrite growth models. The trend of the effective partition coefficient (Fig. 7a) as a function of undercooling is similar to the experimental values but the pseudo-binary approach seems to overestimate the increase in the partition coefficient. This discrepancy highlights the need for non-equilibrium models for dendrite growth of concentrated multi-component alloys [14,42] that will also be found useful by the rapidly growing high entropy alloy community.

Fig. 7b shows the contribution of undercooling as a function of the total undercooling obtained. The effect of curvature and solutal undercooling was prominent up to an undercooling of ~125 K where the dendritic microstructure was prominent. In this domain, the primary dendritic growth was controlled by the diffusion of elements. Above an undercooling of 125 K, the growth was controlled mainly by the collision-controlled growth where the thermal contribution to the undercooling is dominant. This observation is in contrast to the growth of ordered intermetallics and suggests the random solid solution of the primary phase.

2.5. Phase-field simulation

The phase field simulation using multiphase field approach was able to predict the segregation profile as shown in Fig. 8. Here the primary FCC phase is assumed to be a solid solution of Fe, and the diffusion of elements to the Fe was considered for calculation. The Fig. 8 shows the expected segregation pattern, namely, the dendrite phase is rich in Ni and the interdendritic region is mostly Cu. The

Table 3
Values of parameters used in the dendrite growth model.

Kinetic Coefficient (K)	1011	Present work
Super cooling (K)	384	From Thermo-Calc®
Thermal Diffusivity (m^2/s)	$1.7e^{-5}$	Present work
Gibbs–Thomson coefficient (Km)	$2.825e^{-7}$	Present work
Velocity Sound (m/s)	2000	Present work
Partition Coefficient	0.294	From experiment
Composition (at%)	33.333	From experiment
m^0 (liquidus slope) (K/at%)	−2.54	From Thermo-Calc®
Diffusion Velocity (m/s)	5	Present work
Interface Diffusion Velocity (m/s)	5	Present work
Solute Diffusivity (m/s)	$2.24e^{-9}$	Present work

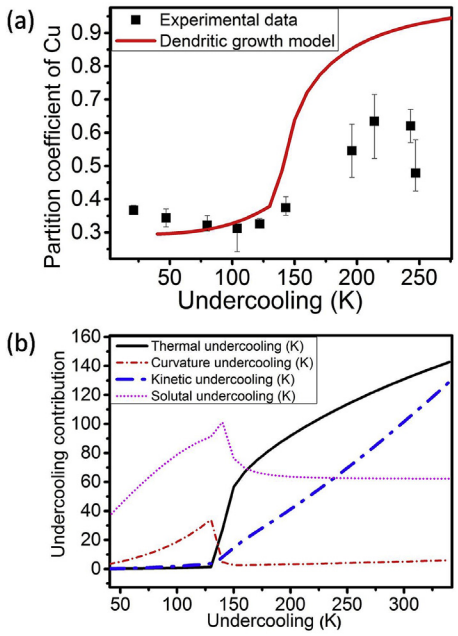

Fig. 7. a) Variation of partition coefficient of Cu as function of undercooling from experiments and pseudo-binary partition coefficient from dendritic growth theory, b) Contribution of different factors in undercooling to the total/bulk undercooling as predicted by dendritic growth theory.

same was also observed in experimental samples. Fig. 8 shows the segregation profiles at undercooling conditions, and it suggests that the nature of elemental segregation is similar in all levels of undercooling. Ni has miscibility with Cu, and its segregation profile shows that enrichment of Ni in the primary phase was limited. Cu has a positive enthalpy of mixing with Fe and its immiscible nature results in segregation in the interdendritic region predominantly. Fig. 9 shows the EDS measurement taken in the solidified sample after an undercooling of 95 K. The virtual EDS show the elemental variation across the interdendritic liquid in the simulated microstructure. The virtual EDS and the experimental EDS scan shows good agreement in the Ni and Cu distribution trend as well as the interdendritic scale for Cu segregation.

Fig. 10a shows the phase field map with increasing extent of undercooling. At this stage, the mobility data for phase field parameter were not calibrated against the experimental growth rates. Hence, a quantitative comparison of the growth rates obtained from phase field simulation with the experimental data was not taken up. An increase in undercooling shows the formation of secondary dendritic arms. At 100 K undercooling, the microstructure formation includes the formation of tertiary dendritic arms too. The comparison of morphology was keeping the numerical parameters such as time step the same. Fig. 10 b shows the phase field simulation result with multiple dendrites which can able to simulate the real microstructure formed during the undercooled condition. The correlation of the simulated and experimental microstructure can be seen from the line EDS taken in the interdendritic region.

There is a close comparison of microstructure and elemental segregation away from the dendrite tip. In equiatomic alloy systems where such segregation could lead to the formation of detrimental intermetallic compounds, these simulations could possibly reduce experimental trials. This can be achieved by performing a follow-up thermodynamic estimate of phase formation on the segregated alloy with compositions taken from the phase field simulations using process conditions that are appropriate for the intended melt

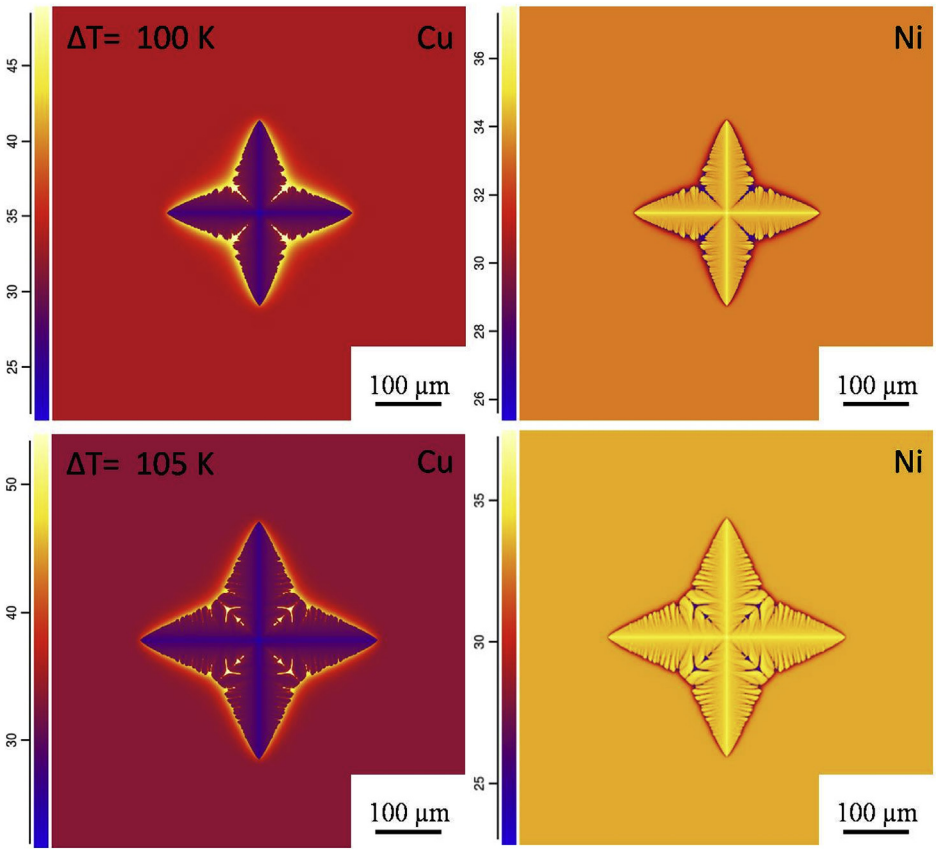

Fig. 8. Simulated segregation patterns of Ni and Cu of undercooled sample of undercooling 100 K and 105 K at a time period of 0.3 s where the colour legends represents the atomic percentage of corresponding elements (simulation details shown in Table 1). (For interpretation of the references to colour in this figure legend, the reader is referred to the Web version of this article.)

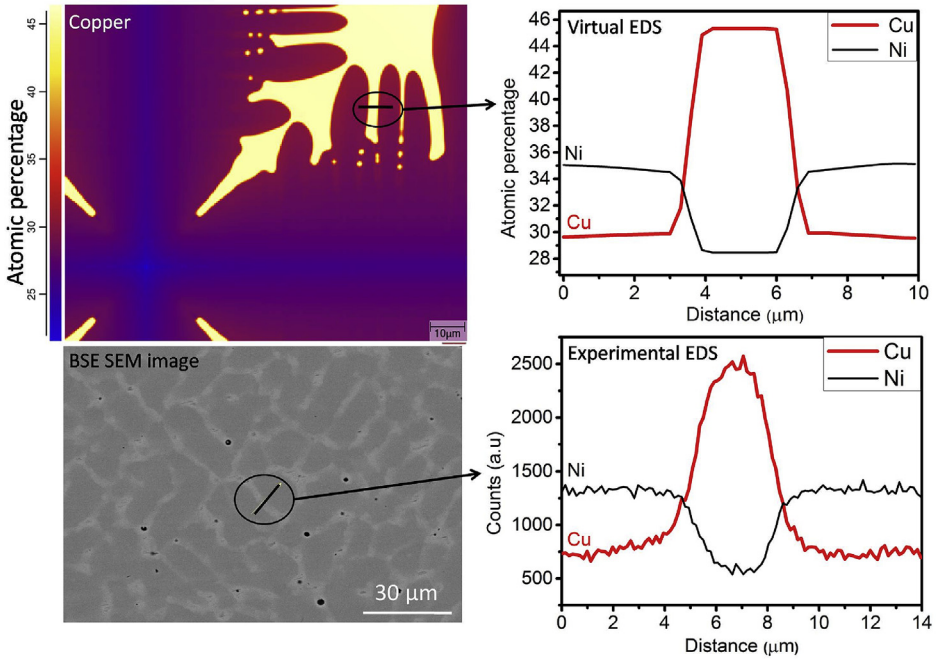

Fig. 9. Line EDS measured from the simulation and experimental sample with an undercooling of 95 K.

processing technique. Segregation is an important aspect that should be brought in as one of the criteria for the design of multi-component equiatomic alloys and high entropy alloys, particularly for processes such as casting, welding, and additive manufacturing.

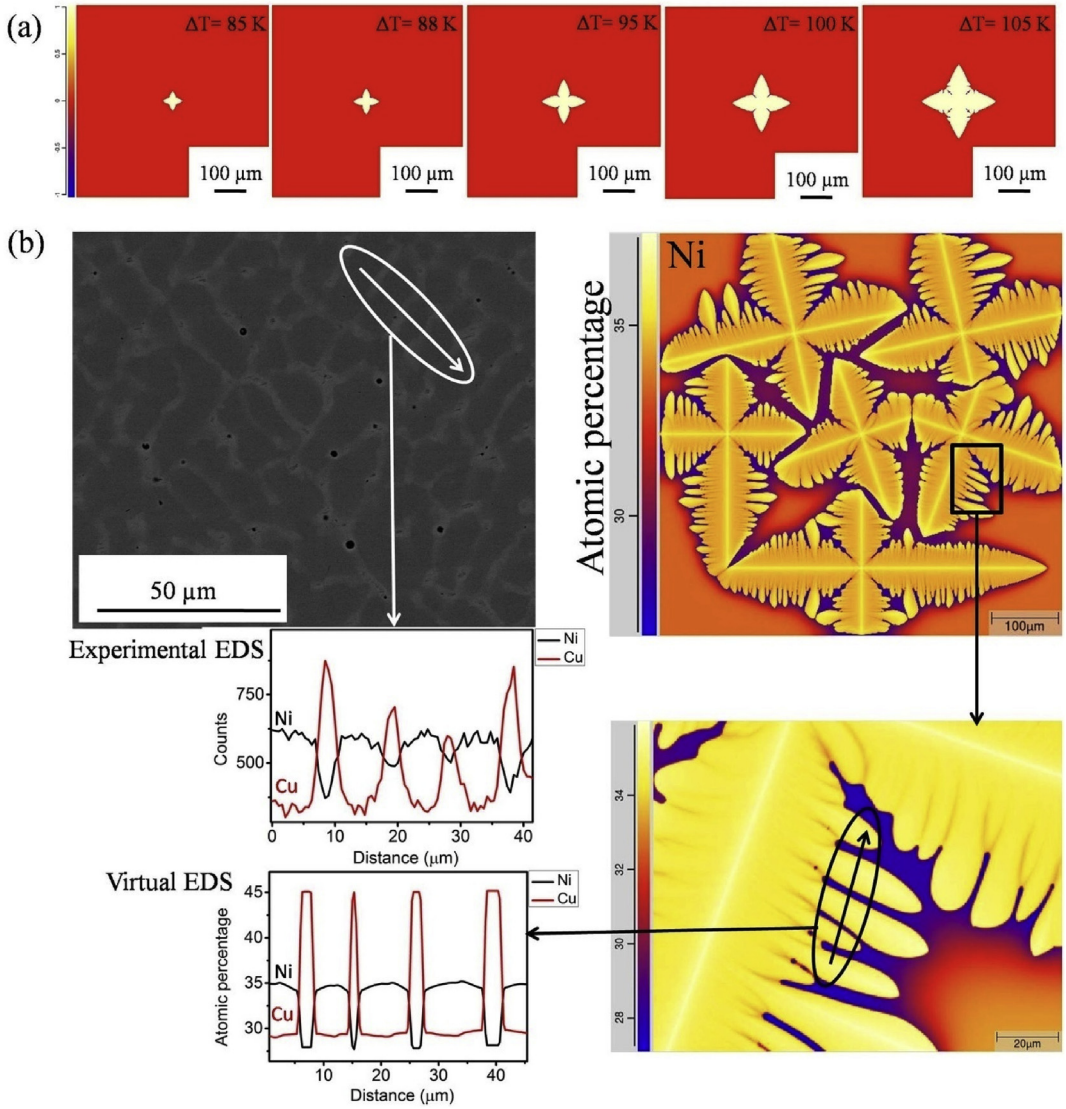

Fig. 10. a) Phase field plots at different undercooling temperatures taken at a solidification time of 0.1 s showing the morphology changes as function of undercooling (simulation details are in Table 1), b) Comparison of microstructure obtained by using multiple dendrite simulation with the experimental micrograph (ΔT = 95 K), the experimental and virtual EDS trends are matching (The simulation was for a solidification time period of 0.9 s).

3. Conclusion

Undercooling studies on Fe–Cu–Ni system shows a transition from dendritic microstructure, equiaxed grain structure, columnar microstructure with increasing undercooling. At an undercooling more than 211 K, the microstructure is characterised by grain morphology. Two types of mechanisms are predominant in grain refinement such as dendritic remelting at lower undercooling regime and recrystallisation or distortion of dendrite at the high undercooling regime. The growth velocity, fitted by a modified dendritic growth model increased nonlinearly with undercooling and the velocity obtained was around 20–30 m/s at 200 K. This confirms that the growth kinetics in this ternary equi-atomic alloy is not sluggish. Partition coefficient indicated solute trapping with increasing undercooling, but segregation of Cu was present even in deep undercooling. The microstructure simulations and segregation profiles compare well with the experiments suggest the applicability of phase field model in equiatomic multi-component systems.

References

[1] Y.J. Kwon, J.W. Won, S.H. Park, J.H. Lee, K.R. Lim, Y.S. Na, C.S. Lee, Ultrahigh-strength CoCrFeMnNi high-entropy alloy wire rod with excellent resistance to hydrogen embrittlement, Mater. Sci. Eng. A 732 (2018) 105–111, https://doi.org/10.1016/j.msea.2018.06.086.
[2] S. Antonov, M. Detrois, S. Tin, Design of novel precipitate-strengthened Al-Co-Cr-Fe-Nb-Ni high-entropy superalloys, Metall. Mater. Trans. A Phys. Metall. Mater. Sci. 49 (2018) 305–320, https://doi.org/10.1007/s11661-017-4399-9.
[3] Z. Li, K.G. Pradeep, Y. Deng, D. Raabe, C.C. Tasan, Metastable high-entropy dual-phase alloys overcome the strength-ductility trade-off, Nature 534 (2016) 227–230, https://doi.org/10.1038/nature17981.
[4] S. Gorsse, C. Hutchinson, M. Gouné, R. Banerjee, Additive manufacturing of metals: a brief review of the characteristic microstructures and properties of steels, Ti-6Al-4V and high-entropy alloys, Sci. Technol. Adv. Mater. 18 (2017) 584–610, https://doi.org/10.1080/14686996.2017.1361305.
[5] A. Munitz, M. Bamberger, A. Venkert, P. Landau, R. Abbaschian, Phase selection in supercooled Cu-Nb alloys, J. Mater. Sci. 44 (2009) 64–73, https://doi.org/10.1007/s10853-008-3115-y.
[6] J. Gao, T. Volkmann, J. Strohmenger, D.M. Herlach, Phase selection in undercooled Nd-Fe-Co-B alloy droplets, Mater. Sci. Eng. A 375–377 (2004) 498–501, https://doi.org/10.1016/j.msea.2003.10.022.
[7] J. Gao, T. Volkmann, D.M. Herlach, Undercooling-dependent solidification behavior of levitated Nd14Fe79B7 alloy droplets, Acta Mater. 50 (2002) 3003–3012, https://doi.org/10.1016/S1359-6454(02)00128-3.

[8] S. Praveen, J.W. Bae, P. Asghari-Rad, J.M. Park, H.S. Kim, Ultra-high tensile strength nanocrystalline CoCrNi equi-atomic medium entropy alloy processed by high-pressure torsion, Mater. Sci. Eng. A 735 (2018) 394–397, https://doi.org/10.1016/j.msea.2018.08.079.
[9] Y. Ikeda, F. Körmann, I. Tanaka, J. Neugebauer, Impact of chemical fluctuations on stacking fault energies of CrCoNi and CrMnFeCoNi high entropy alloys from first principles, Entropy 20 (2018), https://doi.org/10.3390/e20090655.
[10] X.W. Liu, G. Laplanche, A. Kostka, S.G. Fries, J. Pfetzing-Micklich, G. Liu, E.P. George, Columnar to equiaxed transition and grain refinement of cast CrCoNi medium-entropy alloy by microalloying with titanium and carbon, J. Alloy. Comp. 775 (2018) 1068–1076, https://doi.org/10.1016/J.JALLCOM.2018.10.187.
[11] Z. Wu, W. Guo, K. Jin, J.D. Poplawsky, Y. Gao, H. Bei, Enhanced strength and ductility of a tungsten-doped CoCrNi medium-entropy alloy, J. Mater. Res. 33 (2018) 3301–3309, https://doi.org/10.1557/jmr.2018.247.
[12] Y. Ruan, H. Zhu, Q. Wang, F. Dai, D. Geng, B. Wei, Dendrite growth and micromechanical properties of rapidly solidified ternary Ni-Fe-Ti alloy, Prog. Nat. Sci. Mater. Int. 27 (2017) 635–639, https://doi.org/10.1016/j.pnsc.2017.09.004.
[13] G.C. Pettan, C.R.M. Afonso, J.E. Spinelli, Microstructure development and mechanical properties of rapidly solidified Ti–Fe and Ti–Fe–Bi alloys, Mater. Des. 86 (2015) 221–229, https://doi.org/10.1016/j.matdes.2015.07.050.
[14] P.K. Galenko, S. Reutzel, D.M. Herlach, S.G. Fries, I. Steinbach, M. Apel, Dendritic solidification in undercooled Ni-Zr-Al melts: experiments and modeling, Acta Mater. 57 (2009) 6166–6175, https://doi.org/10.1016/j.actamat.2009.08.043.
[15] J. Lipton, M.E. Glicksman, W. Kurz, Dendritic growth into undercooled alloy metals, Mater. Sci. Eng. 65 (1984) 57–63, https://doi.org/10.1016/0025-5416(84)90199-X.
[16] J. Lipton, W. Kurz, R. Trivedi, Rapid dendrite growth in undercooled alloys, Acta 35 (1987) 951–964, https://doi.org/10.1016/0001-6160(87)90174-X.
[17] W.J. Boettinger, S.R. Coriell, R. Trivedi, Application of dendritic growth theory to the interpretation of rapid solidification microstructure, Rapid Solidif. Process. Princ. Technol. 13 (1988).
[18] M.R. Rahul, G. Phanikumar, Design of a seven-component eutectic high-entropy alloy, Metall. Mater. Trans. A 50 (2019) 2594–2598, https://doi.org/10.1007/s11661-019-05210-3.
[19] S. Cazottes, G.Y. Wang, A. Fnidiki, D. Lemarchand, P.O. Renault, F. Danoix, Transmission electron microscopy and X-ray diffraction study of microstructural evolution in magnetoresistive Cu-Fe-Ni ribbons, Philos. Mag. 88 (2008) 1345–1356, https://doi.org/10.1080/14786430802136234.
[20] S.B. Luo, W.L. Wang, J. Chang, Z.C. Xia, B. Wei, A comparative study of dendritic growth within undercooled liquid pure Fe and Fe 50 Cu 50 alloy, Acta Mater. 69 (2014) 355–364, https://doi.org/10.1016/j.actamat.2013.12.009.
[21] P.R. Algoso, W.H. Hofmeister, R.J. Bayuzick, Solidification velocity of undercooled Ni-Cu alloys, Acta Mater. 51 (2003) 4307–4318, https://doi.org/10.1016/S1359-6454(03)00257-X.
[22] W. Yang, F. Liu, H.F. Wang, Z. Chen, G.C. Yang, Y.H. Zhou, Prediction of the maximal recalescence temperature upon rapid solidification of bulk undercooled Cu70Ni30alloy, J. Alloy. Comp. 470 (2009) 13–16, https://doi.org/10.1016/j.jallcom.2008.02.074.
[23] T. Zhang, F. Liu, H.F. Wang, G.C. Yang, Grain refinement in highly undercooled solidification of Ni85Cu15alloy melt: direct evidence for recrystallization mechanism, Scr. Mater. 63 (2010) 43–46, https://doi.org/10.1016/j.scriptamat.2010.03.006.
[24] J.F. Li, Y.C. Liu, Y.L. Lu, G.C. Yang, Y.H. Zhou, Structural evolution of undercooled Ni-Cu alloys, J. Cryst. Growth 192 (1998) 462–470, https://doi.org/10.1016/S0022-0248(98)00399-6.
[25] J.F. Li, W.Q. Jie, G.C. Yang, Y.H. Zhou, Solidification structure formation in undercooled Fe-Ni alloy, Acta Mater. 50 (2002) 1797–1807, https://doi.org/10.1016/S1359-6454(02)00032-0.
[26] R. Sonkusare, A. Swain, M.R. Rahul, S. Samal, N.P. Gurao, K. Biswas, S.S. Singh, N. Nayan, Establishing processing-microstructure-property paradigm in complex concentrated equiatomic CoCuFeMnNi alloy, Mater. Sci. Eng. A 759 (2019) 415–429, https://doi.org/10.1016/j.msea.2019.04.096.
[27] M.R. Rahul, S. Samal, G. Phanikumar, Effect of niobium addition in FeCoNi-CuNb x high-entropy alloys, J. Mater. Res. 34 (2019) 700–708, https://doi.org/10.1557/jmr.2019.36.
[28] S. Samal, M.R. Rahul, R.S. Kottada, G. Phanikumar, Hot deformation behaviour and processing map of Co-Cu-Fe-Ni-Ti eutectic high entropy alloy, Mater. Sci. Eng. A 664 (2016) 227–235, https://doi.org/10.1016/j.msea.2016.04.006.
[29] R.S. Ganji, P. Sai Karthik, K. Bhanu Sankara Rao, K.V. Rajulapati, Strengthening mechanisms in equiatomic ultrafine grained AlCoCrCuFeNi high-entropy alloy studied by micro- and nanoindentation methods, Acta Mater. 125 (2017) 58–68, https://doi.org/10.1016/j.actamat.2016.11.046.
[30] W.L. Wang, L. Hu, S.B. Luo, L.J. Meng, D.L. Geng, B. Wei, Liquid phase separation and rapid dendritic growth of high-entropy CoCrCuFeNi alloy, Intermetallics 77 (2016) 41–45, https://doi.org/10.1016/j.intermet.2016.07.003.
[31] J. Eiken, B. Böttger, I. Steinbach, Multiphase-field approach for multicomponent alloys with extrapolation scheme for numerical application, Phys. Rev. E - Stat. Nonlinear Soft Matter Phys. 73 (2006) 1–9, https://doi.org/10.1103/PhysRevE.73.066122.
[32] B. Böttger, J. Eiken, M. Apel, Multi-ternary extrapolation scheme for efficient coupling of thermodynamic data to a multi-phase-field model, Comput. Mater. Sci. 108 (2015) 283–292, https://doi.org/10.1016/j.commatsci.2015.03.003.
[33] S. Bysakh, K. Chattopadhyay, T. Maiwald, R. Galun, B.L. Mordike, Microstructure evolution in laser alloyed layer of Cu-Fe-Al-Si on Cu substrate, Mater. Sci. Eng. A 375–377 (2004) 661–665, https://doi.org/10.1016/j.msea.2003.10.263.
[34] K.S. Kumar, G. Phanikumar, P. Dutta, K. Chattopadhyay, Microstructural development of dissimilar weldments: case of MiG welding of Cu with Fe filler, J. Mater. Sci. 37 (2002) 2345–2349, https://doi.org/10.1023/A:1015306408611.
[35] S.Y. Shin, S.Y. Han, B. Hwang, C.G. Lee, S. Lee, Effects of Cu and B addition on microstructure and mechanical properties of high-strength bainitic steels, Mater. Sci. Eng. A 517 (2009) 212–218, https://doi.org/10.1016/j.msea.2009.03.052.
[36] S. Takaki, M. Fujioka, S. Aihara, Y. Nagataki, T. Yamashita, N. Sano, et al., Effect of copper on tensile properties and grain-refinement of steel and its relation to precipitation behavior, Mater. Trans. 45 (2004) 2239–2244, https://doi.org/10.2320/matertrans.45.2239.
[37] G.L.F. Powell, The undercooling of Cu-20 wt pct Ag alloy, Tans. Met. Soc. AIME. 245 (1969) 1785.
[38] O. Funke, G. Phanikumar, P.K. Galenko, L. Chernova, S. Reutzel, M. Kolbe, D.M. Herlach, Dendrite growth velocity in levitated undercooled nickel melts, J. Cryst. Growth 297 (2006) 211–222, https://doi.org/10.1016/j.jcrysgro.2006.08.045.
[39] J.E. Rodriguez, C. Kreischer, T. Volkmann, D.M. Matson, Solidification velocity of undercooled Fe-Co alloys, Acta Mater. 122 (2017) 431–437, https://doi.org/10.1016/j.actamat.2016.09.047.
[40] P.K. Galenko, M.D. Krivilyov, Modeling of a transition to diffusionless dendritic growth in rapid solidification of a binary alloy, Comput. Mater. Sci. 45 (2009) 972–980, https://doi.org/10.1016/j.commatsci.2008.12.021.
[41] K. Eckler, R.F. Cochrane, D.M. Herlach, B. Feuerbacher, M. Jurisch, Evidence for a transition from diffusion-controlled to thermally controlled solidification in metallic alloys, Phys. Rev. B. 45 (1992) 5019–5022, https://doi.org/10.1103/PhysRevB.45.5019.
[42] D. Mohan, G. Phanikumar, Experimental and modelling studies for solidification of undercooled Ni-Fe-Si alloys, Philos. Trans. A. Math. Phys. Eng. Sci. 377 (2019) 20180208, https://doi.org/10.1098/rsta.2018.0208.
[43] G. Phanikumar, K. Biswas, O. Funke, D. Holland-Moritz, D.M. Herlach, K. Chattopadhyay, Solidification of undercooled peritectic Fe-Ge alloy, Acta Mater. 53 (2005) 3591–3600, https://doi.org/10.1016/j.actamat.2005.03.053.
[44] M.S. Anand, R.P. Agarwala, Diffusion of copper in iron, J. Appl. Phys. 37 (1966) 4248–4251, https://doi.org/10.1063/1.1708006.